Electrical Measurement of Antiferromagnetic Moments in Exchange-Coupled IrMn/NiFe Stacks

X. Martí,[1,2] B. G. Park,[3] J. Wunderlich,[2,3] H. Reichlová,[2,1] Y. Kurosaki,[4] M. Yamada,[4] H. Yamamoto,[4] A. Nishide,[4] J. Hayakawa,[4] H. Takahashi,[3,4] and T. Jungwirth[2,5]

[1]*Faculty of Mathematics and Physics, Charles University in Prague, Ke Karlovu 3, 121 16 Prague 2, Czech Republic*
[2]*Institute of Physics ASCR, v.v.i., Cukrovarnická 10, 162 53 Praha 6, Czech Republic*
[3]*Hitachi Cambridge Laboratory, Cambridge CB3 0HE, United Kingdom*
[4]*Hitachi Ltd., Advanced Research Laboratory, 1-280 Higashi-koigakubo, Kokubunju-shi, Tokyo 185-8601, Japan*
[5]*School of Physics and Astronomy, University of Nottingham, Nottingham NG7 2RD, United Kingdom*

(Received 8 August 2011; published 3 January 2012)

We employ antiferromagnetic tunneling anisotropic magnetoresistance to study the behavior of antiferromagnetically ordered moments in IrMn exchange coupled to NiFe. Experiments performed by common laboratory tools for magnetization and electrical transport measurements allow us to directly link the broadening of the NiFe hysteresis loop and its shift (exchange bias) to the rotation and pinning of antiferromagnetic moments in IrMn. At higher temperatures, the broadened loops show zero shift, which correlates with the observation of fully rotating antiferromagnetic moments inside the IrMn film. The onset of exchange bias at lower temperatures is linked to a partial rotation between distinct metastable states and pinning of the IrMn antiferromagnetic moments in these states. The observation complements common pictures of exchange bias and reveals an electrically measurable memory effect in an antiferromagnet.

DOI: 10.1103/PhysRevLett.108.017201 PACS numbers: 75.50.Ee, 75.47.−m, 75.70.Cn, 85.80.Jm

Interlayer exchange coupling, giant magnetoresistance, and spin-transfer torque are the three key phenomena that have driven the development of current spintronic technologies [1]. The oldest, yet least understood among the three effects is exchange coupling, especially between an antiferromagnet (AFM) and a ferromagnet (FM) [2,3]. An AFM coupled to a FM can cause broadening of the width H_c of the FM hysteresis loop and the shift H_{eb} of the loop. The AFM/FM exchange bias effect was discovered more than 50 years ago by Meiklejohn and Bean [4]. The authors also proposed the first model of the phenomenon in which a rigid AFM produces a unidirectional exchange field acting on the FM [2–5]. The model tends to overestimate significantly the magnitude of the exchange bias field H_{eb} and fails to describe the simultaneous occurrence of H_{eb} and of the broadening of H_c observed in many AFM/FM exchange-coupled systems. Several theoretical pictures have been proposed to correct for the shortcomings of the Meiklejohn-Bean model by considering, e.g., a domain wall inside the AFM parallel to the AFM/FM interface [6,7], a random exchange interaction due atomic-scale roughness of the AFM/FM interface [8], a domain state with uncompensated spins in the AFM interfacial layer [9], or a spin-glass behavior due to random frustrated interactions at the AFM/FM interface [10].

A detailed understanding of the AFM/FM exchange coupling phenomena requires one to explore experimentally the properties of the AFM. This is, however, notoriously difficult as compared to FMs and relies on experiments at large-scale facilities. For example, neutron diffraction provides an insight into the static spin configuration of different magnetic layers in the AFM/FM stack [2]. Synchrotron-based x-ray linear dichroism experiments on NiO/Co structures are among the very few measurements reported to date which have explored the behavior of AFM moments during magnetization reversal of the coupled FM [11]. In other systems, including the extensively explored stacks with metal exchange biasing AFMs, x-ray linear dichroism has not been reported and the possibility to perform measurements of the AFM films outside large-scale experimental facilities has remained elusive independent of the employed AFM material.

In this Letter, we demonstrate that with common laboratory tools we are able to investigate the behavior of both the FM and the AFM during the magnetization reversal in the archetypical IrMn/NiFe exchange-coupled system [12–16]. Magnetization in the FM NiFe is measured by the superconducting quantum interference device (SQUID). AFM moments in a thin-film IrMn are detected electrically by using the AFM tunneling anisotropic magnetoresistance effect [17]. Measurements reveal a behavior of the AFM spins, correlated with the broadening and shift of the FM hysteresis loop, which is distinct from the previously discussed models of the exchange bias.

Multilayers of SiO_2/Ta(5)/Ru(50)/Ta(5)/$Ni_{0.8}Fe_{0.2}$(10)/$Ir_{0.2}Mn_{0.8}$(1.5, 3)/MgO(2.5)/Pt(10), shown in the inset in Fig. 1, were grown by UHV rf magnetron sputtering in a magnetic field of 5 mT along the flat edge direction of the wafer (layer thicknesses are given in nanometers). Mesa structures of 1×2–5×10 μm^2 for transport measurements were patterned from the wafer by photolithography and ion milling. After device

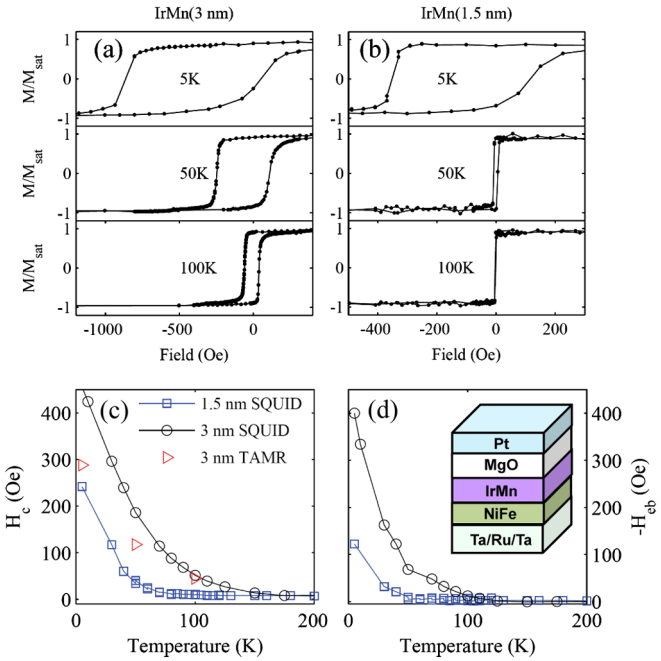

FIG. 1 (color online). SQUID magnetization loops of the 3 (a) and 1.5 nm (b) IrMn samples at 5, 50, and 100 K. (c), (d) Temperature dependence of the width of the hysteresis loop (H_c) and of the shift of the loop (H_{eb}) for the two samples. The inset shows the multilayer structure. The width of the hysteretic region of the tunneling anisotropic magnetoresistance of the 3 nm IrMn sample is shown in (c) for comparison.

fabrication, the wafer was annealed at 350° C for 1 h in a 10^{-6} Torr vaccum in a magnetic field of 0.4 T applied along the same direction as during the growth. Several samples fabricated from each wafer were measured and showed comparable transport characteristics. X-ray diffraction was used to verify the out-of-plane texture of the films; the IrMn and NiFe layers are (111) out-of-plane oriented, and Ru and Ta are (001) and (110) oriented, respectively. In the plane of the layers, the samples are polycrystalline.

In Figs. 1(a) and 1(b), we show magnetization loops measured by SQUID in the 3 and 1.5 nm IrMn wafers at 5, 50, and 100 K. At 100 K, the 1.5 nm IrMn sample shows a very narrow hysteresis loop with coercive field $H_c \sim 10$ Oe, which is similar to the coercivity of the reference NiFe sample without IrMn and is comparable to the error bar of our SQUID measurements. At 50 K, H_c of the 1.5 nm IrMn sample is enhanced, but the hysteresis loop remains centered around zero external field; i.e., H_{eb} is still negligible at this temperature. Only at temperatures below the blocking temperature $T_B \approx 50$ K is the broadening of the loop accompanied by a nonzero shift as seen on the 5 K panel. The magnetization of the 3 nm IrMn sample shows qualitatively the same behavior; only the onset of the broadening of the hysteresis loop occurs at higher temperatures and $T_B \approx 100$ K is also larger in the 3 nm IrMn sample. This is illustrated in Figs. 1(a) and 1(b) and summarized in Figs. 1(c) and 1(d). $H_c > H_{eb}$, and both fields H_c and H_{eb} and the blocking temperature decreasing with decreasing thickness of the AFM film are characteristic features of AFM/FM exchange-coupled systems with ultrathin (< 10 nm) IrMn films [13–15]. Note that, unlike the decreasing blocking temperature with decreasing thickness, previous studies of the Néel temperature showed that the ordering temperature in thin films can be enhanced above the bulk value due to the coupling of the AFM to the FM [18].

Results of our tunneling resistance measurements in transport microdevices with the 3 and 1.5 nm IrMn are shown in Fig. 2. While the SQUID measurements detect the reversal of the FM moments, the tunneling magnetoresistance is sensitive to the change in the orientation of the AFM moments in IrMn. The origin of this transport signal is in the recently discovered tunneling anisotropic magnetoresistance of an AFM/insulator/normal-metal tunnel junction [17]. In analogy to the magnetocrystalline anisotropy or optical linear dichroism, the tunneling anisotropic magnetoresistance is an even function of the microscopic moment and therefore is present equally well for rotating AFM moments as for rotating moments in a FM [17,19]. Since the tunneling resistance is determined by layers adjacent to the tunnel barrier, in our device geometry it corresponds to the reorientation of the AFM moments in IrMn which is in contact with the MgO barrier. The FM moments in the more remote NiFe layer have only an indirect effect on the tunneling transport; they induce via an exchange spring effect [11] the rotation of the AFM

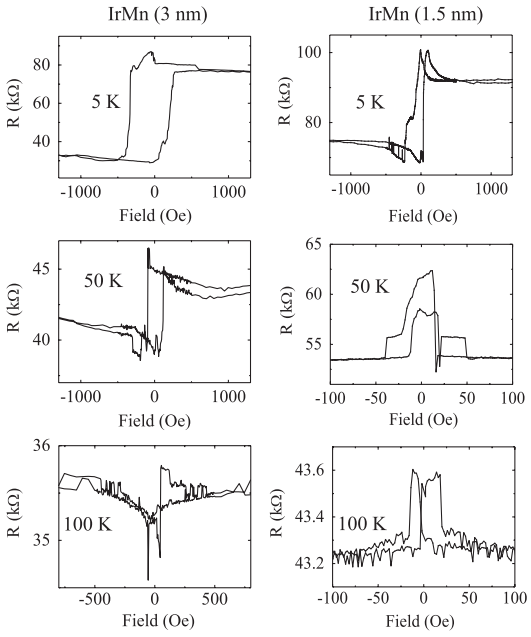

FIG. 2. Tunneling anisotropic magnetoresistance measured as a function of the applied magnetic field strength at the same conditions as the SQUID magnetization loops in Fig. 1.

moments in IrMn during the magnetization reversal of the NiFe [17].

By comparing Figs. 1 and 2, we can draw a direct link between the behavior of FM moments in NiFe and AFM moments in IrMn during the reversal of NiFe. At 100 K, both the 3 and 1.5 nm IrMn samples do not show exchange bias in the SQUID measurements. Corresponding electrical transport measurements show a resistance variation at low fields and the same resistance values at positive and negative saturation fields of the FM. This indicates that the AFM moments also undergo a full 180° rotation which correlates in the SQUID data to the broadened hysteresis loop and zero exchange bias.

Note that in the 1.5 nm IrMn sample, the broadening of the SQUID hysteresis loops starts at temperatures close to 100 K, but at 100 K it is still within the error of the magnetization measurement. The corresponding tunneling magnetoresistance signal is below 1% at 100 K; however, it is clearly detectable. This illustrates the high sensitivity of our transport method for measuring the AFM moments in AFM/FM exchange-coupled systems.

At 50 K, the 3 nm IrMn sample shows a qualitatively different behavior than the 1.5 nm IrMn sample. In the latter sample, the exchange bias is still zero, and, consistently, the resistance values at negative and positive saturation fields of the FM are the same. The absence of the exchange bias is again linked with the full rotation of the AFM moments as was the case of the measurements at 100 K. In the 3 nm IrMn sample, however, H_{eb} measured by SQUID is nonzero at 50 K, and the corresponding tunneling magnetoresistance trace shows different states of the AFM moments at large positive and negative fields. The AFM moments in IrMn make a switch to a different metastable state upon the full reversal of the FM moments in NiFe; however, the AFM rotation angle is not 180°. The same correspondence between shifted magnetization loops of NiFe and asymmetric tunneling resistance traces of IrMn is observed at 5 K for both samples. The signatures of exchange coupling in the FM hysteresis loops are undetectable above ~150 K in the 3 nm IrMn sample and above ~100 K in the 1.5 nm IrMn sample. Consistently, the tunneling anisotropic magnetoresistance vanishes at similar temperatures as the broadening of H_c.

To further support our interpretation of the field-sweep tunneling anisotropic magnetoresistance traces shown in Fig. 2, we performed complementary transport measurements in which the amplitude of the applied field was fixed above the coercive field of NiFe and the magnetic field was rotated by 180°. At this external field strength, the magnetization in NiFe follows the angle of the applied field. IrMn tunneling anisotropic magnetoresistance data recorded in the rotating field are plotted in Fig. 3. They are fully consistent with the picture inferred from the field-sweep measurements in Fig. 2. For example, at 5 K, the resistance values are different at 0° and 180°, and the resistance does not vary over a wide range of intermediate field angles. The AFM moments make a partial rotation and then remain pinned. To highlight the lack of inversion symmetry in the data corresponding to partially pinned AFM moments, we show in Fig. 3 also the inversion symmetry images of the measured field-rotation magnetoresistances. At 100 K, the resistance values are the same at 0° and 180° angles of the applied field. The AFM moments in IrMn make the full 180° rotation, i.e., follow the FM moments in NiFe. At 50 K, the full 180° rotation of the AFM moments is observed only in the 1.5 nm IrMn sample, again consistent with the field-sweep measurements.

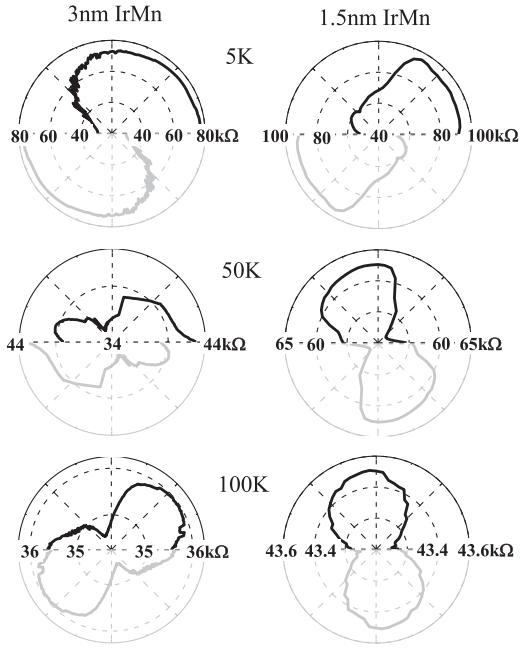

FIG. 3. Tunneling anisotropic magnetoresistance measured (black lines) as a function of the angle of the applied field with magnitude above the coercive field of the NiFe. Gray lines are inversion symmetry images of the measured data.

The Meiklejohn-Bean model [3,5] implies that the exchange bias occurs when $R \equiv K_{\mathrm{AF}} t_{\mathrm{AF}}/J_{eb} \geq 1$, where K_{AF} is the magnetic anisotropy constant in the AFM, t_{AF} is the thickness of the AFM, $J_{eb} = H_{eb} M_F t_F$ is the effective exchange coupling constant at the AFM/FM interface, and M_F and t_F are the magnetization and thickness of the FM, respectively. J_{eb} reaches 0.4 erg/cm^2 (0.4 mJ/m^2) in the 3 nm IrMn sample at low temperatures so that $R \sim 1$ corresponds to $K_{\mathrm{AF}} \sim 10^6$ erg/cm^3. Consistently, the reported magnetic anisotropies in IrMn have typical magnitudes of several times 10^6 erg/cm^3 [20,21]. Since K_{AF} decreases as the temperature increases towards T_N [21], the vanishing H_{eb} observed in our samples at higher temperatures is also qualitatively consistent with $H_{eb} = 0$ in the Meiklejohn-Bean model for $R < 1$. Similarly, the dependence of R on the product of $K_{\mathrm{AF}} t_{\mathrm{AF}}$ can explain the smaller H_{eb} in the 1.5 nm IrMn sample than in the 3 nm

IrMn sample (more so since K_{AF} itself decreases with decreasing thickness in ultrathin IrMn [21]).

The effective interface coupling constant $J_{eb} = H_{eb}M_F t_F$ obtained from the measured H_{eb} is significantly smaller than the exchange constants of the FM or AFM coupled spins in the respective magnetic materials [2,8]. Apart from overestimating the strength of the exchange bias field, the Meiklejohn-Bean model also fails to describe the enhancement of H_c when $H_{eb} \neq 0$. This is because in the model, which considers a uniaxial AFM anisotropy, the AFM moments acquire only a small tilt and then return without hysteresis to the initial state when the 180° FM moment switching is complete. Our AFM tunneling resistance measurements demonstrate that in the presence of the exchange bias the AFM moments rotate to a distinct metastable AFM configuration and remain pinned in that state. The amplitude of >100% of the low-temperature anisotropic magnetoresistance signal indicates that the AFM rotation angle is not small [22]. This combined with the pinning in the intermediate metastable state can explain why the magnitude of the measured exchange bias field is smaller than expected from the Meiklejohn-Bean model. From our data we also see that the rotation of the AFM moments via the metastable states allows for the coexistence of the exchange bias and enhanced coercivity. The AFM shows hysteretic switching during the field sweep in both the presence and the absence of the exchange bias. Consistent with this picture we observe the correlation between the decreasing width of the hysteretic region in the AFM magnetoresistance and decreasing H_c with increasing temperature [compare the field-sweep measurements in Figs. 1(a) and 1(b) and Fig. 2 and see also Fig. 1(c)]. Note that the switching fields are larger and the hysteresis loops are more rounded in the magnetization measurements than in the transport data. The difference is that SQUID measures an average over a large sample area, while the tunneling resistance measurements detect reversal processes in a small area which dominates the tunneling in the transport microdevice. The patterning introduces additional defects which can act as nucleation centers reducing the coercivity.

Our measurements of the AFM tunneling magnetoresistance reveal a picture of the AFM/FM exchange coupling which complements the Meiklejohn-Bean model in a different way than previously discussed in the literature. For example, the models of a domain wall inside the AFM parallel to the AFM/FM interface relate the reduced exchange bias field to the domain wall energy and consider a hysteretic pinning/depinning of the wall during the field sweep [6,7]. The model is unlikely to be applicable to our ultrathin IrMn, whose thickness is much smaller than the expected domain wall width in IrMn [15,23]. Other models [8–10] focus on uncompensated (or frustrated) spins in the interfacial AFM layer in contact with the FM and distinguish a part of these spins which rotate with the FM, and thus enhance H_c, and the part which is fixed and produces H_{eb}. Our transport measurements, on the other hand, are sensitive to the AFM moments at the opposite interface to the one with the FM, and, without distinguishing different types of spins, the observed rotation of the AFM moments via metastable states can be linked to the behavior of both H_c and H_{eb}. Finally, we emphasize that the AFM bistability can be present at zero magnetic field and the corresponding differences in the tunneling resistance can be >100%. Our experiments, therefore, reveal a possibility for realizing memory effects in antiferromagnets which can be detected by large magnetoresistance signals.

We acknowledge support from ERC Advanced Grant No. 268066 0MSPIN, Grant Agency of the Czech Republic No. 109-13/201925 and No. P204/11/P339, and the Charles University No. 443011 and No. SVV-2011-263306, AVCR No. AV0Z10100521, and Preamium Academiae.

[1] C. Chappert, A. Fert, and F. N. V. Dau, Nature Mater. **6**, 813 (2007).
[2] J. Nogués and I. K. Schuller, J. Magn. Magn. Mater. **192**, 203 (1999).
[3] F. Radu and H. Zabel, Springer Tracts Mod. Phys. **227**, 97 (2008).
[4] W. H. Meiklejohn and C. P. Bean, Phys. Rev. **102**, 1413 (1956).
[5] W. H. Meiklejohn and C. P. Bean, Phys. Rev. **105**, 904 (1957).
[6] D. Mauri, H. C. Siegmann, P. S. Bagus, and E. Kay, J. Appl. Phys. **62**, 3047 (1987).
[7] J.-V. Kim and R. L. Stamps, Phys. Rev. B **71**, 094405 (2005).
[8] A. P. Malozemoff, Phys. Rev. B **35**, 3679 (1987).
[9] P. Miltenyi *et al.*, Phys. Rev. Lett. **84**, 4224 (2000).
[10] F. Radu, A. Westphalen, K. Theis-Brohl, and H. Zabel, J. Phys. Condens. Matter **18**, L29 (2006).
[11] A. Scholl *et al.*, Phys. Rev. Lett. **92**, 247201 (2004).
[12] K. Hoshino *et al.*, Jpn. J. Appl. Phys. **35**, 607 (1996).
[13] A. J. Devasahayam and M. H. Kryder, J. Appl. Phys. **85**, 5519 (1999).
[14] M. Takahashi and M. Tsunoda, J. Phys. D **35**, 2365 (2002).
[15] S. Queste *et al.*, J. Magn. Magn. Mater. **288**, 60 (2005).
[16] M. Tsunoda, H. Takahashi, and M. Takahashi, IEEE Trans. Magn. **45**, 3877 (2009).
[17] B. G. Park *et al.*, Nature Mater. **10**, 347 (2011).
[18] P. J. van der Zaag *et al.*, Phys. Rev. Lett. **84**, 6102 (2000).
[19] A. B. Shick *et al.*, Phys. Rev. B **81**, 212409 (2010).
[20] M. J. Carey *et al.*, J. Appl. Phys. **89**, 6579 (2001).
[21] G. Vallejo-Fernandez, L. E. Fernandez-Outon, and K. O'Grady, Appl. Phys. Lett. **91**, 212503 (2007).
[22] The metastable states may originate from magnetic anisotropies in the AFM or from local energy minima corresponding to noncollinear (perpendicular) AFM-FM coupling; N. C. Koon, Phys. Rev. Lett. **78**, 4865 (1997); Y. Ijiri *et al.*, Phys. Rev. Lett. **99**, 147201 (2007).
[23] M. Ali, C. H. Marrows, and B. J. Hickey, Phys. Rev. B **67**, 172405 (2003).